



Comparison of four different models of vortex generators

Fernandez, U.; Réthoré, Pierre-Elouan; Sørensen, Niels N.; Velte, Clara Marika; Zahle, Frederik; Egusquiza, E.

Published in:
Proceedings of EWEA 2012 - European Wind Energy Conference & Exhibition

Publication date:
2012

Document Version
Publisher's PDF, also known as Version of record

[Link back to DTU Orbit](#)

Citation (APA):
Fernandez, U., Réthoré, P-E., Sørensen, N. N., Velte, C. M., Zahle, F., & Egusquiza, E. (2012). Comparison of four different models of vortex generators. In *Proceedings of EWEA 2012 - European Wind Energy Conference & Exhibition* European Wind Energy Association (EWEA).

General rights

Copyright and moral rights for the publications made accessible in the public portal are retained by the authors and/or other copyright owners and it is a condition of accessing publications that users recognise and abide by the legal requirements associated with these rights.

- Users may download and print one copy of any publication from the public portal for the purpose of private study or research.
- You may not further distribute the material or use it for any profit-making activity or commercial gain
- You may freely distribute the URL identifying the publication in the public portal

If you believe that this document breaches copyright please contact us providing details, and we will remove access to the work immediately and investigate your claim.

Comparison of four different models of vortex generators

U. Fernández¹ (unai.fernandez@ehu.es), P.-E. Réthoré² (pire@dtu.dk), N. N. Sørensen² (nsqr@dtu.dk), Clara M. V.² (cmve@dtu.dk), F. Zahle² (frza@dtu.dk) and E. Egusquiza³ (egusquiza@mf.upc.edu).

¹University of the Basque Country, Nuclear Engineering and Fluid Mechanics Department, Nieves Cano 12, 01006 Vitoria-Gasteiz, Araba, Spain

²DTU Wind. AED, Risø, Building VEA 118, Frederiksborgvej 399, DK-4000 Roskilde, Denmark

³Technical University of Catalonia. Fluid Mechanics Department, Av. Diagonal, 647 08028 Barcelona Spain

Abstract

A detailed comparison between four different models of vortex generators is presented in this paper. To that end, a single Vortex Generator on a flat plate test case has been designed and solved by the following models. The first one is the traditional mesh-resolved VG and the second one, called Actuator Vortex Generator Model (AcVG), is based on the lifting force theory of Bender, Anderson and Yagle, the BAY Model, which provides an efficient method for computational fluid dynamic (CFD) simulations of flow with VGs, and the forces are applied into the computational domain using the actuator shape model. This AcVG Model enables to simulate the effects of the Vortex Generators without defining the geometry of the vortex generator in the mesh and makes it easier for researchers the investigations of different vortex generator lay outs. Both models have been archived by the in house EllipSys CFD code using Reynold-Average Navier-Stokes (RANS) methods. The third model is the experimental one, where measurements were carried out in a low speed closed-circuit wind tunnel utilizing Stereoscopic Particle Image Velocimetry (SPIV) with a single vortex generator positioned on a vertical wall in the center of the test section. The fourth model, used as a quantitative comparison, is the analytical model of the primary vortex based in the helical structure of longitudinal embedded vortex, which can reduce the complex flow to merely four parameters:

circulation, convection velocity, vortex core radius and pitch.

The goal of this article is to validate the AcVG Model compared with a fully meshed VG, a wind tunnel experiment and an analytical VG model.

Keywords

Vortex Generators, actuator shape model, CFD, computational fluid dynamics, BAY Model

1. Introduction

A Vortex Generator (VG) is considered as a passive flow control device which modifies the boundary layer fluid motion bringing momentum from the outer region into the inner region. Through this transfer of energy, the velocity of the inner region is increased at the same time as the boundary layer thickness is decreased, which in turn causes the separation of the flow is delayed, Rao et al. [1]. Furthermore, Lin et al. [2] showed the Drag reducing and the Lift increasing effect of sub boundary layer VGs.

Vortex Generators are applied on wind turbine blades with the major aim to delay or prevent the separation of the flow and to decrease roughness sensitivity of the blade. They are usually mounted in a spanwise array on the suction side of the blade and have the advantage that they can be added as a post-production fix to blades that do not perform as expected. So, adding VGs is a

simple solution to improving the performance of a rotor, Schubauer et al. [3] and Bragg et al. [4].

In order to design a wind turbine blade, and to optimize the position of the VGs on the blade, Computational Fluid Dynamics (CFD) tools can be used. However, modelling the fully-meshed VGs on a full rotor computation becomes prohibitively expensive. Indeed, the Vortex Generators size is often similar to the boundary layer thickness and many small cells are needed in the VG geometry in order to have a reliable modelling of the flow. An alternative way of modelling VGs in CFD is to model the influence of the vortex generator on the boundary layer using body forces.

Bender et al. [5] developed a source term model based on the Joukowski lift theorem and thin airfoil theory, called the BAY Model. This model was presented for simulating vane Vortex Generators in a finite volume the Navier-Stokes code that eliminates the requirement to define the geometry in the mesh. For the calibration of the model, a test case was created by [5] for comparison of the results with a modelled VG and the gridded VG. This test case consisted in a pipe with 24 VGs mounted circumferentially in a co-rotating configuration. The study showed to promising results.

Subsequently, a new improved version of the BAY model was developed by A. Jirásek [6], called jBAY Model. This new version was

based on the lift force theory of [5] and provided a more capable method for simulating the flow with rows of VGs. Jirásek [6] used a simplified technique for defining the model control points, so in this way it was easier to implement the model and the results were more accurate. The model was tested with a single VG on a flat plate, in an S-Duct air intake in a high-lift wing configuration. The results showed very good agreement between experimental data and CFD computations. Afterwards, an empirical model of VGs was incorporated into the Wind-US Navier-Stokes CFD code by Dudek [7] and in 2011 a simplified implementation was developed by Dudek [8]. With the implementation of the BAY model in the CFD code, the effects of the VGs using fine mesh are simulated by adding lift forces in the region of cells at the VG position. With this simplification the reduction of mesh cells can reach 30% of the fine mesh needed with a resolved VG, Wallin [9].

2. Models Description

Four VG Models have been performed in this work for a detailed comparison, both qualitative and quantitatively. In order to carry out this comparison, a test case based on a single VG in a flat plate was designed. The proposal of this research has been divided as Figure 1 shows.

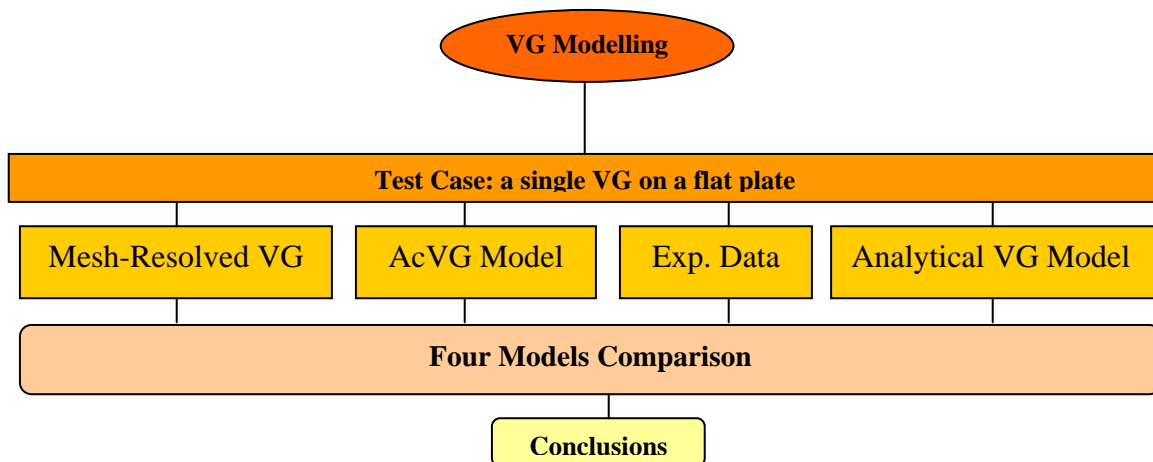


Figure 1: Test Case Layout

The computations of the first two models, mesh-resolved VG and AcVG model, were performed using the EllpSys CFD code Michelsen [10] and Sørensen [11], which is an in house structured finite-volume CFD package for the numerical simulations of flows using Reynolds-Averaged Navier-Stokes equations

These two CFD methods are compared with a wind tunnel experiment. In this experiment, a parametric study was performed over a single vane placed on the test section wall in a low-speed wind tunnel. The flow was recorded using Stereoscopic Particle Image Velocimetry, in cross-planes at various positions downstream of the vane, providing instantaneous three-component realizations throughout the measurement plane. This enables an overview of the averaged downstream development of the wake, including both velocity field and streamwise vorticity, suitable for comparison with computations. The experimental conditions and setup are the same as described in Velte et al. [12].

Finally an analytical model of the primary vortex is considered in the context of the two CFD models and the wind tunnel experiment. The model described in this work, which can reduce the complex flow to merely four parameters (circulation, convection velocity, vortex core radius and pitch), enables quantitative comparison in addition to the qualitative one, Velte [13].

In every test case the measurements have been conducted in a spanwise plane, in a plane normal to the flat plate, positioned five VG heights downstream of the vortex generator.

2.1 Mesh-Resolved VG Model.

This model consists in a single VG on a flat plate and the computational domain has been defined with the following normalized dimensions with the VG height, as shown in the Figure2. The flow domain width is 30 times the VG height and the height is 5 times. The flow domain length is 32 times the VG height in order to capture the generated vortex.

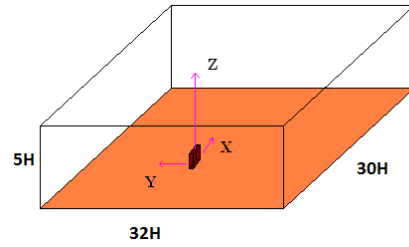


Figure 2: Computational domain of mesh-resolved VG Model.

The geometry dimensions of the rectangular VG are defined with a length of two times the VG high, see Figure 3. The thickness of the vane is constant and with no sharp edges. A boundary layer is developed over the flat plate, forced by the viscous interaction between the wall and the flow. The VG was positioned in the flat plate in such way that the boundary layer thickness at this location is equal to the VG high.

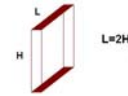


Figure 3: VG Dimensions.

The angle of attack defined is 20 degrees, see Figure 4. and the Shear Stress Transport SST turbulence model has been chosen due to its ability to solve swirling flows Liu et al. [18]

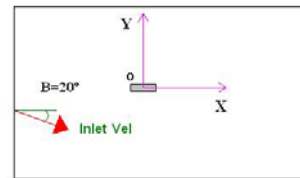


Figure 4: Angle of attack.

The Reynolds Number based on VG height is:

$$Re = \frac{\rho u_{\infty} H}{\mu} = 833 \quad (2.1)$$

The computational setup of the fully-meshed VG Model consists in a block structured mesh of 18 million cells with the large part of them used to capture the vortex generated downstream the VG, Figure 5. Five levels of mesh size have been defined for this model

and a mesh dependency of less than 5% has been detected.

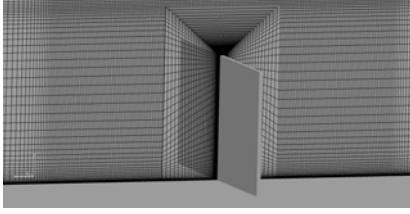


Figure 5: Mesh Section on the VG.

2.2 Actuator VG Model.

In the wind turbine, VGs are often used to improve the performance of the blades by minimizing the effects of the boundary-layer separation and the adverse pressure gradients. So, computational fluid dynamics (CFD) methods are used to simulate the flow and to predict the blade performance. Together with experiments in wind tunnel, it is a very useful tool for parametric studies of VG lay-out, however, these CFD methods are very time consuming in the computations and in generating a high level quality mesh.

In this work we introduce the Actuator Vortex Generator Model (AcVG) based on the Bay Model, developed by Bender et al. [5]. The main idea of the BAY Model is to replace the VG geometry by a subdomain at the original VG location and to apply the force distribution in this region, as shown in figure 6. The influence of the VG onto the flow is modelled through a source term normal to the local velocity.

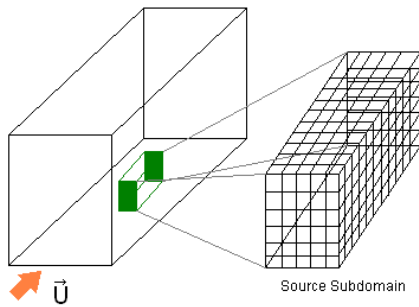


Figure 6: BAY Model source subdomain on a flat plate.

The BAY Model incorporates a source term in the momentum and/or energy equations where VGs are taken in account through the body forces exerted on a fluid.

$$V_i \frac{\Delta(\rho u)}{\Delta t} = \sum_j FM_j S_j + Li \quad (2.2)$$

$$V_i \frac{\Delta(\rho E)}{\Delta t} = \sum_j FE_j S_j + uLi \quad (2.3)$$

The source term applies a force normal to the local flow direction, parallel to the surface which simulates the side force generated by a VG.

$$Li = c_{vg} S_{vg} \frac{V_i}{\sum V_i} \alpha \rho u^2 \hat{l} \quad (2.4)$$

The variable u is the local velocity, α is the angle of the incidence of the vane, V_i is the volume of the grid cell and $\sum V_i$ is the sum of the cells where the model is applied. ρ is the local density, S_{VG} is the area of the VG and c_{VG} is an empirical constant for calibration. So, in the Actuator VG Model a parametric analysis was performed to determinate a reliable value of c parameter and validated with the mesh-resolved VG Model. The Figure 7 shows that for the value of the total force of the mesh-resolved VG Model ($f = 3.32e^{-2}$) is corresponding to a c_t value of 2.2.

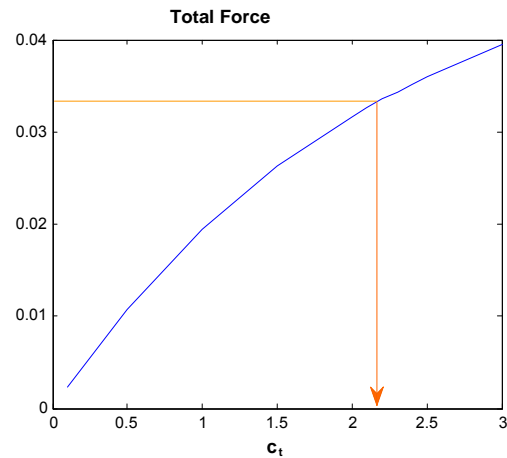


Figure 7: Calibration of the c_t parameter..

A Mesh dependence study for Actuator VG Model has been performed with 3 different levels of grid. Results from the fine mesh are compared with the results with the course and medium mesh, Figure 8.

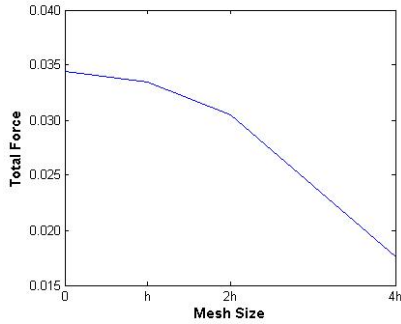


Figure 8: Mesh Dependency plot.

The procedure has been achieved by using the Richardson Extrapolation Method for a mesh dependency study, Stern et al [15]. Three parameters are calculated in the Richardson Extrapolation: p , R and RE , the order of accuracy, the error ratio and the extrapolated solution respectively. A fine, medium and coarse mesh are defined with the corresponding mesh sizes h_1 , h_2 and h_4 . A mesh dependency around 2% has been detected.

The innovation of this research is that instead of applying forces in all cells of the subdomain, as the BAY Model, the force is applied in cells just in the outline of the VG geometry, see figure 2. The forces are applied into the computational domain using the actuator shape model presented in Réthoré et al. [16]. The body forces are applied in the domain using a modified Rhie-Chow algorithm presented in Réthoré and Sørensen [17], using the EllipSys CFD code, Michelsen [10] and Sørensen [11]. The Actuator VG Model has been designed to be user-friendly. Within the EllipSys CFD code, the user only specifies the following parameters for each VG to be modelled: the cells where the model will be applied and the angle of the incidence of the VG.

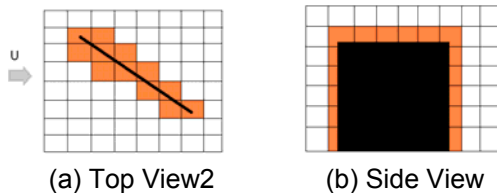


Figure 10: Cells where the forces are applied.

2.3 Experimental Data Model.

Consider the test section setup in Figure 11, the measurements were carried out in a closed-circuit wind tunnel with an 8:1 contraction ratio and a test section of cross-sectional area 300 × 600 mm with length 2 m. At the inlet of the test section, a turbulence-generating grid with mesh length 39 mm was situated.

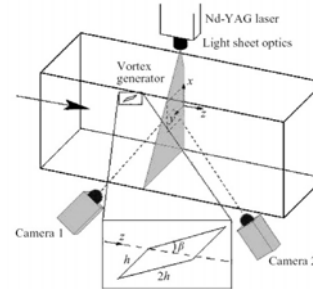


Figure 11: Schematic illustration of the experimental set-up and device geometry. The large arrow to the left indicates the main flow direction and β the device angle. The measurement plane in the laser sheet has been indicated by dashed lines.

The experiments were conducted at free stream velocity $U_\infty = 1.0 \text{ m s}^{-1}$. The wind tunnel speed was obtained by measuring the pressure drop across an orifice plate. The turbulence intensity at the inlet from laser doppler anemometry (LDA) measurements has been found to be 13 %. The boundary layer thickness at the position of the vortex generator has been estimated from LDA measurements to be approximately $\delta_{VG} = 25 \text{ mm}$. The actuator, as seen in Figure 11, is a rectangular vane of the same height as the local boundary layer thickness, $h = \delta_{VG}$, with a length of $2h$. The vortex generator was positioned on a vertical wall in the center of the test section with its trailing edge 750 mm downstream of the inlet grid when it is at zero angle to the mean flow.

The measurements were conducted in a spanwise plane, with plane normal parallel to the test section walls, positioned five device heights downstream of the vortex generator. The measurement plane has been indicated by a dashed line in Figure 11.

The SPIV equipment was mounted on a rigid stand and included a double cavity New Wave Solo 120XT Nd-YAG laser (wavelength 532 nm) capable of delivering light pulses of 120 mJ. The pulse width, i.e., the duration of each illumination pulse, was 10 ns. The light-sheet thickness at the measurement position was 2 mm and was created using a combination of a spherical convex and a cylindrical concave lens. The equipment also included two Dantec Dynamics HiSense MkII cameras (1344 × 1024 pixels) equipped with 60 mm lenses and filters designed to only pass light with wavelengths close to that of the laser light.

2.4 Analytical VG Model.

The existence of Lamb-Oseen reminiscent vortex structures embedded in wall bounded flow has been reported in various experiments and numerical simulations, Liu et al. [18]. For the Lamb-Oseen vortex, the vorticity is non-zero only for the axial component as

$$\omega_r = 0; \quad \omega_\theta = 0; \quad \omega_z = \frac{\Gamma}{\pi a^2} \exp\left(-\frac{r^2}{a^2}\right) \quad (2.5a-c)$$

A more general model is the Batchelor vortex [19], which includes the non uniform axisymmetrical axial velocity distribution u_z which approaches the Lamb-Oseen vortex in the extreme. This vortex model is commonly used in instability studies of swirling flows Heaton et al.[24]. To describe experimental swirl flows the Batchelor vortex model is usually referred to in the form:

$$u_\theta = \frac{K}{r} (1 - \exp(-\alpha r^2)) \quad (2.6 a)$$

$$u_z = W_1 + W_2 \exp(-\alpha r^2) \quad (2.6 b)$$

where K , W_1 , W_2 and α are empirical constants with simple physical interpretations as identified by Okulov [20]

$$\Gamma = 2\pi K \quad (2.7 a)$$

$$l = K/W_2 \quad (2.7 b)$$

$$u_0 = W_1 + W_2 \quad (2.7 c)$$

$$\varepsilon = 1/\sqrt{\alpha} \quad (2.7 d)$$

where Γ is the vortex strength (circulation), l is the pitch of the helical vortex lines, u_θ is the advection velocity of the vortex and ε is the effective size of the vortex core with Gaussian axial vorticity distribution (see Figure (12)).

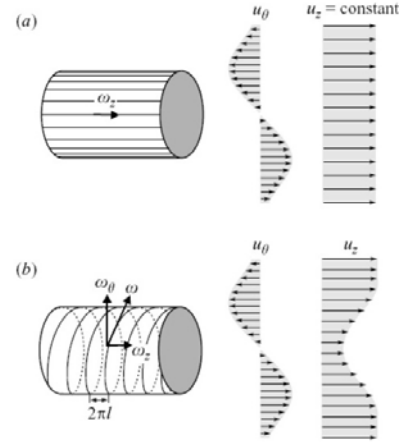


Figure 12: Sketch of vorticity field and induced velocity profile by Lamb-Oseen vortex with rectilinear vortex lines (a) and Batchelor vortex with helical structure of vortex lines (b).

The profiles given in (2.6) can reproduce experimentally determined swirl flow with high accuracy. One possible approach is to test if the empirical model (2.6) can describe the longitudinal vortex in the present case. However, in accordance with Pierrehumbert [23] one needs to account for the possible disturbance of the mirror vortex, resulting from the presence of the wall. Another more suitable approach is therefore to extend the Batchelor vortex model to model the flow by helical symmetry of the vorticity, leaving no restrictions on the shape of the vortex core. Flows with helical vorticity can be described by correlation between the axial and circumferential vorticity vector components:

$$\omega_r = 0 \quad (2.8 a)$$

$$\omega_\theta = r\omega_z/l \quad (2.8 b)$$

$$\omega_z = \frac{\Gamma}{\pi\varepsilon^2} \exp\left(-\frac{r^2}{\varepsilon^2}\right) \quad (2.8 c)$$

with the vorticity vector always directed along the tangent of the helical lines $x = r \cos \theta$; $y = r \sin \theta$; $z = l\theta$. Flows with helical vorticity can in addition be characterized by the following condition for the velocity field:

$$u_z + \frac{r}{l}u_\theta = u_0 \equiv \text{constant} \quad (2.9a,b)$$

$$u_z = u_0 - \frac{r}{l}u_\theta \quad (2.9a,b)$$

it can be shown that conditions (2.8a,b) and (2.9) are equivalent (Okulov [21]). For a flow fulfilling the requirement of (5.5), the main flow parameters are u_0 and l . Sometimes u_0 , u_z and u_θ are found directly from measurements. The pitch l can then be deduced from (2.9), but this approach might lead to an estimate of high relative error if $u_z - u_0$ is small. Multiplying (2.9) by u_z and integrating over the cross-section of the flow one can obtain the pitch through the swirl number S , Alekseenko et al. [22])

$$l = \frac{-F_{mm}}{(F_m - u_0 G)} \quad (2.10)$$

where $F_{mm} = \int \Sigma \rho u_z r d\Sigma$ is the angular momentum flux in the axial direction, $F_m = \int \Sigma \rho u_z z d\Sigma$ the momentum flux in the axial direction, G the flow rate, ρ the fluid density and Σ the cross-section area. All parameters can now be determined: u_0 is found directly from the measurements, l is found through (5.6) and the circulation Γ and the vortex size ε can be extracted from (5.4c).

Based on the experimental observation the simple Batchelor vortex model is chosen as

$$u_\theta = \frac{\Gamma}{2\pi r} \left[1 - \exp\left(-\frac{r^2}{\varepsilon^2}\right) \right] \quad (2.7 a)$$

$$u_z = u_0 - \frac{\Gamma}{2\pi l} \left[1 - \exp\left(-\frac{r^2}{\varepsilon^2}\right) \right] \quad (2.7 b)$$

The only requirements of this simple model are the size of the vortex core, the circulation, the helical pitch and the vortex advection velocity.

3. Models Comparison.

Results of a single gridded VG on a flat plate and the AcVG Model were performed using the EllipSys CFD code. Figures 13(a) and (b) show the evolution of the vortex downstream of the VG for the mesh-resolved VG Model and for the AcVG model respectively.

3.1 Qualitative Comparison

For a qualitative comparison between the mesh-resolved VG Model and the AcVG Model, four parameters have been chosen: pressure, axial velocity, vorticity and turbulent kinetic energy. All of these fields have been taken at the calibration distance of five VG heights downstream the trailing edge of the VG and plotted in the Figure 14.

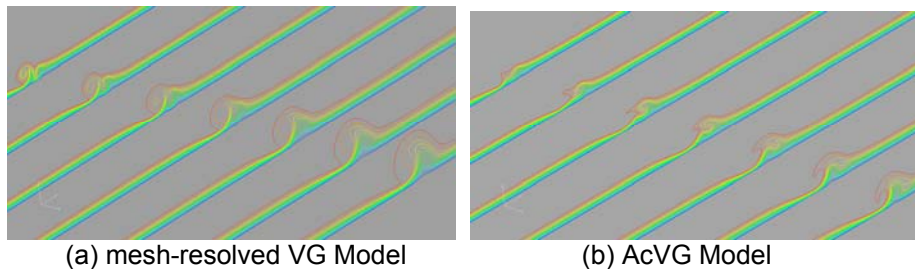
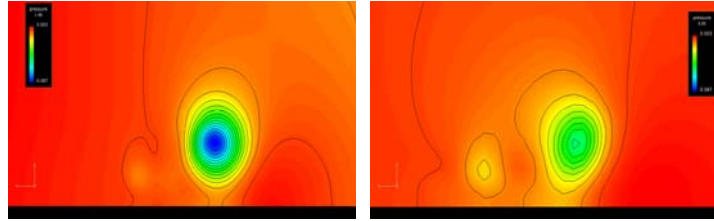
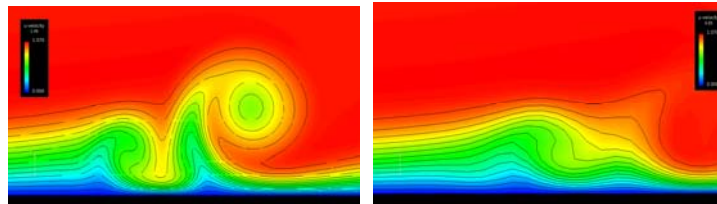


Figure 13: CFD results of a single VG on a flat plate. Down stream Vortex Development

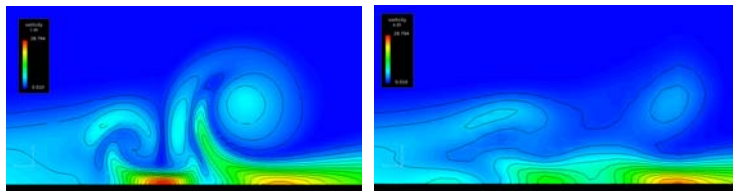
Fields for qualitative comparison:



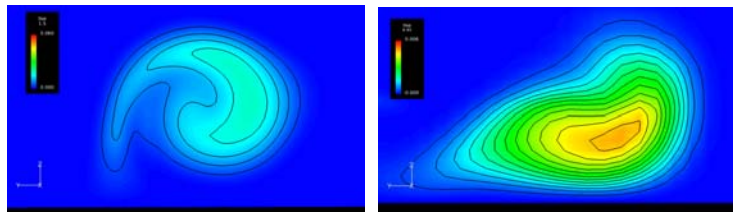
(a): Pressure



(b): Axial Velocity



(c): Vorticity Fields



(d): TKE

Figure 14: Fields for qualitative comparison. Mesh resolved VG Model on the left and AcVG Model on the right. (a) Pressure Fields, (b) Axial Velocity Fields, (c) Vorticity Fields, (d) Turbulent Kinetic Energy.

3.2 Quantitative Comparison

As a quantitative comparison, an analytical model of the primary vortex is considered in the context of the two CFD models (mesh-resolved Vg and AcVG Models) and the wind tunnel experiment. This Analytical Model described in Velte [13]., reduces the complex flow to four parameters (circulation, convection velocity, vortex core radius and helical pitch) and enables quantitative comparison in addition to the qualitative one,

Figure 15 shows the axial u_z (upper) and azimuthal u_θ (lower) velocity profiles for a 20 degrees of the device angle and extracted along a line parallel to the wall through the center of the primary vortex.

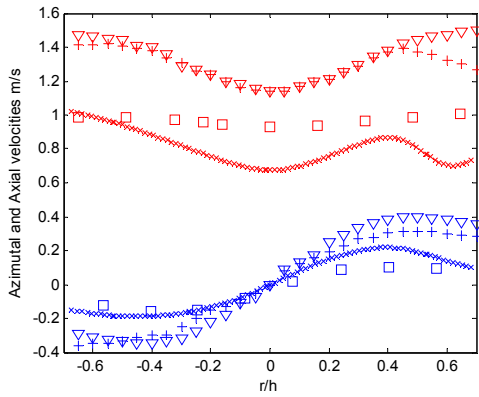


Figure 15 Comparison of axial and azimuthal velocities of embedded vortices generated by a vortex generator for a device angle of 20 degrees. (x) mesh-resolved VG Model, (□) Actuator VG Model, (+) Experimental data Model, (v) Analytical VG Model. Upper values (red colour) are the axial velocity profile u_z and lower (Blue colour) the azimuthal velocity profile u_θ .

In order to analyse the quantitative differences between the results of the four models, the Root Mean Square Error RMSE has been calculated

$$RMSE = \sqrt{\frac{\sum_{i=1}^n (a_{1,i} - a_{2,i})^2}{n}}$$

Figure 16 shows the differences between the models, having as a reference the Actuator

VG Model. Green colour bars illustrate the axial velocity differences and the yellow ones the azimuthal differences. M1, M2 M3 and M4 represent the four models: mesh-resolved VG, AcVG, experimental data and the Analytical Model respectively. So, M2-Mi symbolizes the difference between the AcVG Model and the “i” Model.

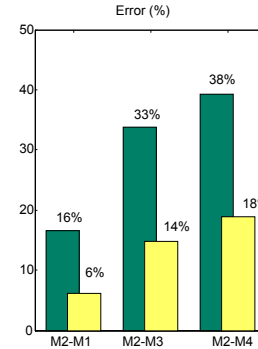


Figure 16: Differences of the four models in the axial (green) and the azimuthal (yellow) velocities.

More plots have been calculated for a quantitative comparison based in the Analytical VG Model’s parameters defined in Velte [13]: vortex core radius circulation, helical pitch and advection velocity

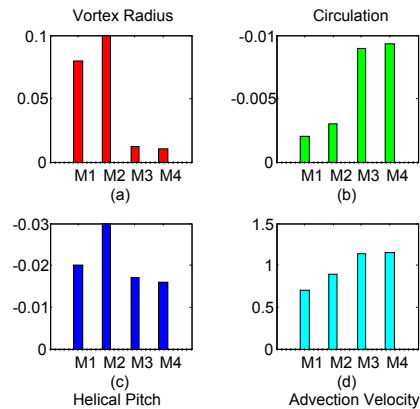


Figure 17: Comparison plots of the parameters: (a) Vortex radius, (b) Circulation, (c) helical pitch and (d) advection velocity. M1, M2 M3 and M4 represent the models: mesh-resolved VG, AcVG, experimental data and the Analytical Model respectively.

4. Results

Results of the calibrated Actuator VG Model have compared with the mesh-resolved VG Model, the experimental data and the Analytical Model. Significant differences have been observed between the four models. The deviations between the values of the Actuator VG Model and the values predicted by the analytical model are quite important, also with the values of the experimental data.

In regard to the computational time, the mesh-resolved VG Model time has been estimated in 1080 hours using 36 CPUs; however the Actuator VG Model only 3.2 hours, using 16 CPUs. So from the point of view of the computational effort, the efficiency of the AcVG Model is much higher than the mesh-resolved VG. Also a significant reduction in cells is achieved by replacing the detailed VG boundary layer mesh by the new modelling method. This mesh reduction decreases both the VG geometry meshing time and the computational time. These results show that AcVG and mesh-resolved VG Models are qualitatively similar. Once vortex produced by the mesh-resolved VG is fully developed at around 10 VG heights downstream the trailing edge of the VG, the AcVG Model matches the vortex generated by the mesh-resolved VG Model. Figure 13 shows a good agreement in the sense of the vortex development. However; some discrepancies are visible in the quantitative comparison, above all in the axial velocity. It might be because the vortex development at the calibration plane is not completed. As the Figure 16 shows, the most important divergences of the models in comparison with the Actuator VG Model are located in the axial velocity

Also, some discrepancies are visible on the amount of turbulence kinetic energy generated between the fully meshed VG model and the AcVG Model, which produces less turbulence, as it can be expected from this type of source term model.

5. Discussion

The discussion focuses on the physical property of the new AcVG model, compared with the fully meshed model, the wind tunnel experiment and the analytical model. What are the compromises done in terms of physics, with this new model?

6. Conclusions

In conclusion, a new model has been implemented in the EllipSys CFD code and demonstrated that it saves both meshing and computational time. This method could easily be applied for complementing full rotor computation and for doing parametric study of the VG layout. The potentially open applications of the Actuator VG Model are several.

Also, we can confirm that the analytical model developed by [14] can be used as a calibration tool for the AcVG Model

• Acknowledgements

The author would sincerely like to thank the researchers of DTU Wind at the Technical University of Denmark contributed to this work and to the Centre for Industrial Diagnosis and Fluid Dynamics CDIF at the Technical University of Catalonia.

References

- [1] Rao D. M., Kariya TT. Boundary-layer submerged vortex generators for separation control—an exploratory study. AIAA Paper 88-3546-CP, AIAA/ASME/SIAM/APS 1st National Fluid Dynamics Congress, Cincinnati, OH, July 25–28, 1988.
- [2] Lin, S. K. Robinson and R. J. McGhee. Separation Control on high-lift airfoils via micro vortex generators. *Journal of aircraft*, 27(5):503-507, 1994.
- [3] Schubauer G. B., Spangenberg W. G. Forced mixing in boundary layers. *J Fluid Mech*, 1 1960;8:10–32.
- [4] Bragg M. B. Gregorek GM. Experimental study of airfoil performance with vortex generators. *J Aircr* 1987; 24(5):305–9.
- [5] Bender, E. E., Anderson, B. H., and Yagle, P. J., “Vortex Generator Modeling for Navier–Stokes Codes,” American Soc.of Mechanical Engineers Paper FEDSM99-6929, New York, July 1999.
- [6] Jirásek A. Vortex-Generator Model and Its Application to Flow Control. *JOURNAL OF AIRCRAFT* Vol. 42, No. 6, Swedish Defence Research Agency FOI, SE-172 90 Stockholm, Sweden, 2005
- [7] Dudek J. Empirical Model for Vane-Type Vortex Generators in a Navier–Stokes Code *AIAA JOURNAL* Vol. 44, No. 8. NASA Glenn Research Center, Brookpark, Ohio 44135, August 2006.
- [8] Dudek J. Modelling Vortex Generators in a Navier–Stokes Code. NASA John H. Glenn Research Center at Lewis Field, Cleveland, Ohio 44135. *AIAA JOURNAL* Vol. 49, No. 4, April 2011
- [09] Wallin, F. Flow control and shape optimization of intermediate turbine ducts for turbofan engines. PhD thesis, Chalmers University of Technology, Gothenburg, Sweden, 2008.
- [10] Michelsen J.A. Basis3d- a platform for development of multiblock pde solvers. Technical Report AFM 94-06, Technical University of Denmark, Dept. of Mechanical Engineering, 1994.
- [11] Sørensen N. N. General purpose flow solver applied to flow over hills. Technical Report Risoe-R-827(EN), Risoe National Laboratory, 1995.
- [12] Velte, C.M., Hansen, M. O. L., Okulov, V. L., ”Helical structure of longitudinal vortices embedded in turbulent wall-bounded flow”, *J. Fluid Mech.*, 619, 167 – 177, 2009.
- [13] Velte C. M. Characterization of Vortex Generator Induced Flow. PhD Thesis, Technical University of Denmark, Lyngby, Denmark 2009.
- [14] Allan B.G., Yao C-S and Lin J.C. Simulation of embedded streamwise vortices on a flat plate. Technical report, National Aeronautics and Space Administration, May 2002
- [15] Stern F., R.V. Wilson, H.W. Coleman and E.G. Paterson. Verification and validation of the CFD simulations. Technical report, The University of Iowa, September 1999.
- [16] Réthoré P.-E., Sørensen N. N., Zahle F., Validation of an actuator disc model. EWEC 2010 conference proceedings. 2010.
- [17] Réthoré P.-E., Sørensen N. N. A discreet force allocation algorithm for modeling wind turbines in CFD. *Wind Energy Journal*. Accepted for publication. 2011.

- [18] Liu, J., Piomelli, U. & Spalart, P. R. 1996 Interaction between a spatially growing turbulent boundary layer and embedded streamwise vortices. *Journal of Fluid Mechanics* 326, 151_179.
- [19] Batchelor, G. K. 1964 Axial flow in trailing line vortices. *Journal of Fluid Mechanics* 20, 645_658.
- [20] Okulov, V. L. 1996 The transition from the right helical symmetry to the left symmetry during vortex breakdown. *Technical Physics Letters* 22, 798_800.
- [21] Okulov, V. L. 2004 On the stability of multiple helical vortices. *Journal of Fluid Mechanics* 521, 319_342.
- [22] Alekseenko, S. V., Kuibin, P. A., Okulov, V. L. & Shtork, S. I. 1999 Helical vortices in swirl flow. *Journal of Fluid Mechanics* 382, 195_243.
- [23] Pierrehumbert, R. T. 1980 A family of steady, translating vortex pairs with distributed vorticity. *Journal of Fluid Mechanics* 99, 129_144.
- [24] Heaton, C. J. & Peake, N. 2007 Transient growth in vortices with axial flow. *Journal of Fluid Mechanics* 587, 271_301.